New austalide derivative from the marine-derived Aspergillus sp. and evaluation of its biological activity

Mohamed S. Elnaggar
Ain Shams University
Ahmed M. Elissawy (aelissawy@pharma.asu.edu.eg)
Ain Shams University
Fadia S. Youssef
Ain Shams University
Abdel Nasser B. Singab
Ain Shams University

Article

Keywords: Aspergillus sp, Caco-2 cells, COVID-19, Molecular docking, Meroterpenoids, NMR

Posted Date: May 11th, 2022

DOI: https://doi.org/10.21203/rs.3.rs-1602654/v1

Abstract

Chemical investigation of the ethyl acetate extract of *Aspergillus sp.* isolated from the soft coral *Sinularia* species resulted in the isolation of one new meroterpenoid austalide X (**1**), one known austalide W (**2**), six known prenylated indole diketopiperazine alkaloids (**3-8**) and phthalic acid and its ethyl derivative (**9-10**). The structures were established using 1D and 2D NMR experiments supported by UV analysis and ESI-MS (Electrospray ionization mass spectrometry). The effect of changing the fermentation media was also investigated using LC-PDA-MS (Liquid chromatography-photodiode-array-mass spectrometry) employing rice and beans media. It showed significant quantitative and qualitative variations particularly in the diketopiperazine content. *In vitro* cytotoxic evaluation was performed using MTT assay. Results showed that the examined compounds revealed weak to moderate activities where the new meroterpenoid, austalide X (**1**) displayed IC_{50} value of 51.6 µg/mL. *In silico* molecular docking was done to evaluate COVID-19 inhibitory potential of isolated compounds on 2019-nCoV main protease, spike glycoprotein and Angiotensin-Converting Enzyme 2 (ACE2). Compound **(10)** followed by compound **(9)** exerted a potent inhibition on all the examined proteins with high fitting scores. ADME/TOPKAT (absorption, distribution, metabolism, excretion, and toxicity) predication performed *in silico* showed that most of the isolated compounds revealed reasonable pharmacokinetic, pharmacodynamic and toxicity properties.

1. Introduction

Kingdom Fungi constitutes a prolific source of bioactive compounds where plethora of drug products has been developed from fungal metabolites since the discovery of penicillin from *Penicillium notatum* by Sir Alexander Fleming in 1928. These drugs comprises the antihyperlipidemic agents atorvastatin and simvastatin, the antifungal drug griseofulvin, the anti-migraine drug ergotamine as well as the immunosuppressant drug cyclosporine [1].

Basically, endosymbiotic fungi colonize in the inner tissues of a host, either plant or animal [2], exhibiting mutual benefits, where the host organism provides a proper medium for the growth of the fungus and in turn the growing fungal species provides the host with bioactive compounds enabling it to survive unfavorable conditions [3] and mediating the different ecological interactions [4]. Endosymbiotic fungi derived from marine ecosystems had received much attention in the last two decades with the isolation of more than one thousand fungal species from marine habitats [5]. Cephalosporin C was the first bioactive molecule isolated from marine derived fungus *Cephalosporium sp*. [6] and since then endosymbiotic fungi had proven to be a fabulous source of bioactive secondary metabolites belonging to different classes such as terpenoids [7, 8], diketopiperazines [9], polyketides [10, 11], benzophenones [12], peptides [13] and butyrolactones [14].

Meroterpenoids represent a major class of fungal terpenoids [7, 15-17] meanwhile austalides represent a unique class of polycyclic (tetra-, penta- hexa- or heptacyclic) meroterpenoids with isobenzofuranone moiety. Thirty-four members of austalides were mainly isolated from different *Penicillium* and *Aspergillus* species demonstrating potential activities including anti-osteoporosis, antibacterial, antiviral, cytotoxic and

α-glucosidase inhibitory activity [18-23]. Moreover, many synthetic approaches had been reported for different members of the austalide family [24-26].

Noteworthy to highlight that cancer and infectious diseases triggered by viruses, bacteria and fungi still represent a major impendence in the progress of therapeutic approaches to improve public health. The recent development of COVID-19 infection badly affects people all over the globe causing severe respiratory disorder accompanied by pneumonia, hyperinflammation, hyperferritinemia, hemophagocytic and lymphohistiocytosis. Thus, it was urgent to search for effective naturally occurring drug entities to combat these challenges that are less expensive possessing less adverse effect compared to synthetic agents [27].

In continuation of our ongoing search of new secondary metabolites from marine derived fungi, we herein reported the chemical investigation of the ethyl acetate extract of the fungus *Aspergillus sp.* isolated from the inner tissues of the soft coral *Sinularia* sp. collected from the coast of Sharm El-Sheikh, Egypt. We herein reported the isolation and characterization of one new meroterpenoid austalide X (**1**), one known austalide W (**2**) in addition to six known prenylated indole diketopiperazine alkaloids (**3-8**) along with phthalic acid and its ethyl derivative (**9-10**) (Figure 1)**.** All isolated compounds were assessed for their cytotoxic effect against Caco-2 cells using MTT assay. In addition, *in silico* evaluation of their COVID-19 inhibitory potential was done using molecular docking within the active center of on 2019-nCoV main protease, 2019-nCoV spike glycoprotein and Angiotensin-Converting Enzyme 2 (ACE2) downloaded from protein data bank. Besides, prediction of the pharmacokinetic and pharmacodynamic potential as well as the toxicity properties of the isolated compounds was performed using ADME/TOPKAT protocol in Discovery Studio 4.5 (Accelrys Inc., San Diego, CA, USA).

2. Results And Discussion

2.1. Chemical investigation of the ethyl acetate extract of the fungus Aspergillus sp.

In depth chemical investigation of the ethyl acetate extract of the fungus *Aspergillus sp.* isolated from the inner tissues of the soft coral *Sinularia* sp. collected from the coast of Sharm El-Sheikh, Egypt resulted in the isolation and characterization of one new meroterpenoid austalide X (1), one known austalide W (2) [18] in addition to six known prenylated indole diketopiperazine alkaloids (3-8) [28, 29] along with phthalic acid and its ethyl derivative (9-10).

Compound (1) was isolated as a pale-yellow amorphous powder. LC-ESI-MS revealed a pseudomolecular ion peak at *m/z* 505 and 503representing $[M+H]^+$ and $[M-H]^-$ respectively, (supplementary S1) and corresponds to the molecular formula $C_{26}H_{32}O_{10}$. UV spectrum of compound (1) showed a characteristic pattern of austalides with λ_{max} at 270 nm. Its chemical structure was elucidated through 1D and 2D NMR spectroscopic analysis (supplementary S2-S7), alongside with the reported data for the related analogues austalides V and W [18]. Analysis of ^1H and APT-NMR spectra displayed a close similarity between compound (1) and austalide W (2), where, APT spectrum (Table 1) revealed the presence of 26 carbons, including one carbonyl group, six olefinic or aromatic carbons and thirteen aliphatic carbons, one tri-

oxygenated quaternary carbon, one di-oxygenated quaternary carbon , three oxygenated quaternary carbons, one quaternary aliphatic carbon, one oxygenated methine carbon, one aliphatic methine carbon, two oxygenated methylene carbons, three aliphatic methylenes, two methoxyl carbons and four methyls.

Meanwhile, ^{1}H NMR spectrum of compound (1) (Table 1) displayed two methine protons at δ_H (ppm) 3.80 (1H, *dd*, *J* = 5.5, 0.9 Hz , H-18) and 3.05 (1H, *dd*, *J* = 7.5, 1.8 Hz, H-21) in which the former is oxygenated, in addition to five methylene protons at δ_H (ppm) 5.14 (2H, *s*, H-1), 4.16, 3.95 (2H, *d*, *J* = 9.7Hz, H-25), 2.95 (2H, *m*, H-22), 2.64, 2.39 (2H, *d*, *J* = 14.5 Hz, H-12) and 2.15, 1.85 (2H, *dd*, *J* = 15.9, 0.9 Hz; 15.9, 5.5 Hz, H19) in which the former two methylenes are oxygenated in addition to the presence of two methoxyl protons at δ_H (ppm) 4.16 (3H, *s*, OMe-29) and 3.53 (3H, *s*, OMe-28). Besides, four methyl protons at δ_H (ppm) 2.06 (3H, *s*, Me-23), 1.69 (3H, *s*, Me-26), 1.35 (3H, *s*, Me-24) and 0.87 (3H, *s*, Me-27) were observed.

The above-mentioned data were found to be in complete accordance with the reported data for austalides class [30-32] in which one known analogues of this group of compounds was also isolated here in our study from the same crude extract, namely austalide W (2) [30]. Compound (2) was found to be in close similarity to the structure of compound (1), moreover, it is worthy to highlight that compound (2) was previously reported to be the first austalide derivative having a 5/6/6/6/6/5/5 heptacyclic ring system including a tetrahydrofuranyl ring [30]. In addition, this ring system arrangement was confirmed also in compound (1) to be in alignment with all previously reported austalides, as well as the affirmation of presence of ring G through the existence of the down-fielded CH_2 group (C-25) at δ_H (ppm) 4.16, 3.95 (2H, *d*, *J* = 9.7 Hz) and δ_C (ppm) 78.2, alongside with the existence of a characteristic down-field carbon shift of C-13 at δ_C (ppm) 102.0, in which all those characteristic shifts found to be are similar to compound (2) [30] affirming the presence of the unusual tetrahydrofuranyl ring (ring G) in the structure of compound (1).

By inspection of the NMR data mentioned above for compound (1), it was clear that it differs from austalide W (2) only by the presence of a newly added hydroxyl group at C-18, this hydroxylation is unambiguously deduced through the difference molecular weight of both compound by only 16 units to the molecular weight of compound (1) than compound (2). Moreover, in COSY spectrum, there is a distinct correlation between H-18 and H_2-19 confirming the adjacent positioning of both groups. This suggestion was further confirmed through inspection of the reported data for compound (2), in comparison to the data of the newly isolated compound (1), in which instead of the methylene group at C-18 in compound (2), a clearly observed oxygenated methine proton was detected at δ_H (ppm) 3.8 on C-18. Hence, there is a low field chemical shift from δ_H (ppm) 1.81-1.94 in compound (2) [30] to δ_H (ppm) 3.8 in compound (1) as well as a low field shift of carbon from δ_C (ppm) 30.92 in compound (2) [30] to δ_C (ppm) 69.2 in compound (1), in addition a low field shift is also detected in APT NMR for C-19 from δ_C (ppm) 30.83 in compound (2) [30] to δ_C (ppm) 37.7 in compound (2), side by side with confirmatory HMBC correlations from the newly observed methine proton H-18 to δ_C 39.2 (C-20) and δ_C 118.5 (C-17) alongside with correlations from δ_H (ppm) 0.87 (H_3-27) and δ_H (ppm) 2.15, 1.85 (H_2-19) towards δ_C (ppm) 69.2 (C-18). It is noteworthy to mention that Antipova et al. had isolated an acetylated derivative, austalide V, where the oxygenated methine was placed at C-19, in our case HMBC correlations had affirmed the

presence of the oxygenated methine at C-18 instead, as revealed by the absence of strong correlations between the methyl protons of C-27 and the oxygenated methine carbon C-18. Thus, compound (1) must possess a heptacyclic skeleton as other austalide analogues. Hence, the planar structure of (1) was elucidated as shown, for which the trivial name austalide X is proposed.

The relative configuration of those stereocenters included within compound (1) was determined based on NOESY NMR data (Figure 2). A key NOESY correlation between methyl protons at C-26 and C-27 suggested that ring G to be in an *exo*-position as well as the *endo*-configuration of the OH group located at C-13, similarly to other previously reported austalide analogues [30]. Meanwhile, the NOE correlations of methyl protons on C-24 with methine proton at C-21 indicate that both rings C & D are being on the same plane in a *cis*-connection. In addition, the observed cross-peak correlations between the oxygenated methine proton on C-18 with the methine proton at C-21 alongside with an obvious absence of any cross-peaks or correlations with the former proton with either C-26 or C-27, supposed the *endo*-position of the OH group on C-18.

Moreover, according to the previously reported possible biosynthetic pathway which suggested that they were all originated from the parent 6-[(2*E*,6*E*-(farnesyl]-5,7-dihydroxy-4-methylphthalide followed by cyclization and oxidative modification, and thus all austalide members were originated the same way [30]. Additional proposed pathway was reported as another trial performed by Paquette for austalide derivatives in which he reported a full synthesis of austalide B, one of the austalide group of compounds, [33, 34]. Thus, those two reported proposed pathways declared that there is a constancy of carbon atom's configuration among all austalide group members and suggested having the same stereochemistry at the specified stereocenters. Hence, the absolute configuration of the stereocenters of compound (1) in our study here is coincidence with all other reported austalide derivatives to be 11S*, 13S*, 14S*, 15S*, 17S*, 18R*, 20S*, 21R*.

2.2. Effect of OSMAC approach on secondary metabolites obtained from the ethyl acetate extracts of the fungal strain

Applying OSMAC approach through changing the fermentation culture medium from the conventional solid rice culture medium to solid beans culture medium was investigated. The ethyl acetate extract of *Aspergillus* sp. obtained from both media was analyzed using LC-PDA-MS. and revealed apparent changes in their UV and MS profiles. From PDA (photodiode array) data it was clearly obvious that major differences both in qualitative and quantitative manner of the secondary metabolites were observed among the two extracts. Figures 3 and 4 illustrate the HPLC/PDA chromatograms recorded at 254 nm and at maximum absorbance 200-400 nm of both extracts. Major peaks existing in both extracts were compared in (table 2) and different peaks were written in italics where λ max., retention times, area % and peak number of the relevant peaks were displayed. For simplification, the comparison included in table 2 had been performed for detection in channel one at 254 nm. Both positive and negative ESI-MS modes of relevant peaks were merged with the PDA data and included in table 3. From merged PDA and MS data, it was concluded that the major effect of changing the culture media was the complete disappearance of the major compounds produced in the original fermentation medium (i.e., Rice medium) at retention time

32.8 min. (18%) and 35.7 min. (21%) when using beans alternatively as a culture media. These two compounds with molecular weights 511 and 479 respectively, corresponding to compounds (3) and (4) (diketopiperazine derivatives), had been isolated and identified. Moreover, the new meroterpenoid, austalide X (1), with molecular weight 504 and λ max 270 nm, was found in both extracts, indicating no significant effect of the culture media on its production by the fungal isolate. Additionally, peak at retention time 22.7 min produced in rice medium with λ max 251, 290 nm, had been disappeared in the beans medium. This peak corresponds to the spiro-diketopiperazine (8) with molecular weight 427.

2.3. In vitro cytotoxic evaluation of the isolated compounds using MTT assay

Cytotoxic evaluation of compounds (3), (4), (6), (8) (diketopiperazine derivatives) as well as compounds (1) and (2) (meroterpenoid derivatives) against Caco-2 (human colorectal carcinoma cell lines) revealed weak to moderate activities displaying IC_{50} values ranging between 32.5 and 126 µg/mL where the new meroterpenoid, austalide X (1) displayed substantial cytotoxic effect with IC_{50} of 51.6 µg/mL as illustrated in table 4.

2.4. In silico molecular docking to evaluate COVID-19 inhibitory potential of isolated compounds

In silico molecular docking was performed on three critical proteins involved in the growth, replication, and invasive character of SARSCoV-2 virus namely 2019-nCoV main protease 2019-nCoV spike glycoprotein and Angiotensin-Converting Enzyme 2(ACE2) (Table 5). Noteworthy to highlight that protease enzyme plays an important role in the process of protein maturation in many viruses *via* cleansing proproteins after being translated into host cell cytosol. Thus inhibition of viral proteases could serve as therapeutic targets for antiviral agents *via* reduction of mature viral particles assembly [35]. Meanwhile, S glycoprotein is crucially important in the process of virus attachment, fusion and entrance within the host cell acting as the main target for host immune system *via* neutralizing the antibodies. Thus, S glycoprotein serves as the main target vaccine preparation and in many therapeutic approaches [36]. Besides, the effectiveness of binding of SARS viral spike (S) protein with ACE2 was elucidated and turned to play the main role in SARS-CoV transmissibility. Hence, the inhibition of ACE2 catalytic pocket using bioactive drug leads could change ACE2 conformation so that it effectively prevents the entrance of SARS-CoV into the host cells [27].

Results displayed in Table 5 revealed that compound (10) followed by compound (9) highly inhibited all the examined proteins with high fitting scores. Compound (10) showed binding energy (ΔG) equals = -25.20 kcal/mole with 2019-nCoV main protease active site owing to the formation of four conventional H-bonds with Asp187, Arg188, Gln189 in addition to the formation of two π-alkyl bonds with Met165 and Met49, one C-H bond with Asp187 and many Van der Waals interactions with the amino acid residues present at the active center (Figure 5A). However, Compound (10) greatly inhibited 2019-nCoV spike glycoprotein displaying high fitting score (ΔG = -12.17 kcal/mole) exceeding that of 2019-nCoV spike glycoprotein co-crystalized ligand that showed ΔG of -2.61 kcal/mole. This mainly attributed to the formation of firm three H-bonds with Thr236 and Asn234 in addition to the formation of C-H bond with Thr236 and Van der Waals interaction with Thr108 (Figure 5B). Regarding ACE2, compound (10)

displayed the highest fitting within its active site with (ΔG = -15.86 kcal/mole) showing superior fitting when compared to ACE2 co-crystalized ligand (ΔG = -6.65 kcal/mole). This firm fitting can be interpreted by the virtue of formation of three conventional H-bonds with Ala193, His195, Asn194 in addition to the formation of C-H bond with His195 and Van der Waals interaction with Val107 and Asn103 (Figure 5C).

2.5 ADME / TOPKAT prediction

Prediction of the pharmacokinetic and pharmacodynamic potential as well as the toxicity properties of the isolated compounds was performed using ADME/TOPKAT protocol in Discovery Studio 4.5 (Accelrys Inc., San Diego, CA, USA). Regarding human intestinal descriptor,
compounds (1), (2), (4), (7), (8) (9) and (10), showed good human intestinal absorption level and thus they lie within the 99% absorption ellipse as displayed in ADMET plot (Figure 6). Concerning the solubility level, compound (10) showed optimal solubility while the rest of compounds revealed possible or good solubility levels. Compounds (4), (9) and (10) revealed medium to low BBB penetration level and thus lie inside the 99% BBB confidence eclipse in ADMET plot (Figure 6). On the contrary, the rest of compounds have undefined BBB penetration level taking level 4 and lies outside the 99% BBB confidence eclipse. Regarding the binding of compounds with plasma protein, compounds (3-8) and (10) displayed less than 90% PPB while the rest of compounds showed more than 90% PPB. Additionally, all of the isolated compounds showed no inhibition to CYP2D6 but some of the compounds showed certain hepatotoxic effect as compounds (3-8) and (10) (Table 6).

Regarding TOPKAT prediction, all the examined isolated compounds displayed no mutagenicity as predicted by chemical *Ames* mutagenicity protocol done *in silico*. Furthermore, most of the compounds showed no carcinogenic effect to both male and female rat (NTP) except for compounds (9-10) for female rat and compounds (1-2) and (6-8) for male rats. They displayed rat oral LD50 values between 0.16-9.68 g/kg-body-weight with compounds (9-10) showed the highest LD50 of 9.68 and 4.05 g/kg-body-weight, respectively. Similarly for the rat chronic LOAEL level, all the isolated compounds displayed values between 0.0017-1.6549 g/kg-body-weight with compounds (9-10) showed the highest LOAEL of 0.9889 and 1.6549 g/kg-body-weight, respectively. Regarding skin irritancy, most of the isolated compounds showed no to mild skin irritation. For ocular irritation, most of the isolated compounds showed no to mild skin irritation except compound (6-8) and (10) that showed moderate eye irritation. Thus, it can be concluded that most of the isolated compounds showed reasonable pharmacokinetic, pharmacodynamic and toxicity properties so could be incorporated in pharmaceutical dosage forms to prevent cancer and combat COVID-19 infection. Additionally, compounds (9) and (10) that showed the highest fitting scores revealed the best pharmacokinetic and pharmacodynamic properties with slight toxicity that can be controlled by the given doses when formulated in pharmaceutical preparations (Table 7).

3. Experimental Section

3.1. General experimental procedures

NMR spectra (chemical shifts in ppm) were recorded on a Bruker AVANCE HD III 400 MHz spectrometer (Switzerland). NMR samples were dissolved in methanol-d_4 or chloroform-d_3, (Sigma Aldrich, Germany) and transferred to 3 mm NMR tubes (Bruker). LC-PDA-MS analyses were performed using Shimadzu LCMS 8045 system coupled with photodiode array detector (LC-2030/2040) with detection wavelengths of 235, 254 and 280 nm with λ max absorption at 220-400 nm. LC-PDA-MS was equipped with RP-C18 UPLC column (shimpack 2 mm × 150 mm) possessing 2.7 µm particle size using the following gradient elution (Acetonitrile (ACN), 0. 1% HCOOH in H_2O) 0-2 min (10% MeOH); 2-35 min (10% ACN-100% ACN) and 35-40 (100% ACN) with 0.2 mL/min flow rate. Final purification steps were performed using preparative HPLC (Shimadzu, Japan) using Kromasil C-18RP semi-preparative column (10 mm × 250 mm) at a flow rate of 5 mL/min and UV detection at wavelength of 254 nm with λ max absorption at 220-400 nm. Medium pressure liquid chromatography was performed on Puriflash 4125 system equipped with PDA detector. Normal phase column chromatography was performed using silica gel 60 (0.04-0.063, Merck, Germany). TLC analyses were performed using normal phase silica gel pre-coated plates F_{254} (Merck, Germany). All the consumed solvents were of analytical grade meanwhile those used for HPLC analyses are of HPLC grade.

3.2. Fungal material

The fungus *Aspergillus sp.* was isolated from the inner tissues of the marine soft coral *Sinularia.* The soft coral was collected from the Red Sea close to Sharm El-Sheikh, Egypt, in September 2018 at 5-7 meters depth. For isolation of the fungal strain the soft coral was rinsed with distilled water and then surface sterilization was performed using 70% ethanol for 2 min. Small samples from the inner tissues of the soft coral were aseptically cut using sterilized blade and pressed onto malt agar plate (15 g/L malt extract, 15 g/L agar, 0.2 g/L chloramphenicol to suppress bacterial growth, pH adjusted to 7.4-7.8 using 10% NaOH). After incubation at 25°C the fungal strain under investigation was found to grow out of the sponge tissue. Pure fungal strains were grown by repeated re-inoculation on fresh culture media.

3.3. Identification of the fungal strain

The isolated fungal strain was identified as *Aspergillus* sp. using a molecular biological protocol by DNA amplification and sequencing of the ITS region as previously reported [37]. The obtained data of sequencing were submitted to GenBank with the accession number OK035701.

3.4. Cultivation, extraction, and isolation

Small scale fermentation of the fungal strain was performed on solid rice culture media (100 g Rice in 110 mL distilled water, autoclaved for 20 min at 121°C) in 1L Erlenmeyer flask (2 flasks were used). Simultaneously, small scale fermentation was performed on solid beans medium (100 g beans in 110 mL distilled water, autoclaved for 20 min at 121°C) in 1L Erlenmeyer flask (2 flasks were used), both cultures were incubated for 30 days at 25 °C under static conditions. Large scale fermentation was performed on solid rice medium using 12 Erlenmeyer flasks (1L each). Fungal cultures were extracted using ethyl acetate

(EtOAc), the combined extracts were then evaporated *in vacuum* and the residue was partitioned between *n*-hexane and 90% aqueous methanol yielding about 3 grams of reddish-brown solid residue**.**

The defatted extract was then applied to vacuum liquid chromatography (VLC) packed with normal phase silica gel as stationary phase applying stepwise gradient as follows 80% *n*-hexane in ethyl acetate to 100% ethyl acetate, followed by dichloromethane in methanol from 95% to 50%. Eluted fractions were analyzed using TLC and similar fractions were pooled together yielding 7 major fractions (FR1-7). Fraction FR3 (500 mg) was fractionated using normal phase medium pressure liquid chromatography eluted with linear gradient elution from 80% *n*-Hex:EtOAc to 30% *n*-Hex:EtOAc. Final purification was performed using RP-semi-preparative HPLC, eluted with linear gradient elution from 70% ACN: H_2O to 95% ACN: H_2O with final purification of two compounds **(3)** (25 mg) and **(4)** (30 mg)**.** Fraction FR4 (350 mg) was directly applied to semi-preparative HPLC and subsequently eluted with linear gradient elution from 50% ACN:H_2O to 90% ACN:H_2O yielding compounds (**1)** (9mg), (**5)** (15 mg) and (**10)** (? 30 mg). Fraction FR5 (700 mg) was fractionated using normal phase medium pressure liquid chromatography (puriflash®) eluted with linear gradient elution from dichloromethane: Methanol gradient (from 100% to 80%) yielding three major sub-fractions FR5-V1- FR5-V3. Fraction FR5-V1- was purified using RP-semi-prep-HPLC-PDA eluted with linear gradient elution from 20% ACN:H_2O to 60% ACN:H_2O yielding compounds (**2)** (12 mg) and (**9)** (20 mg). Similarly fraction FR5-V3 was purified using semi-prep HPLC and eluted using 30% ACN:H_2O to 60% ACN:H_2O yielding compounds (**6)** (11 mg), (**7)** (7 mg) and (**8)** (4 mg).

3.5. Compound characterization

Austalide X (**1**): Pale-yellow amorphous powder. ^{1}H (400 MHz) and ^{13}C (100 MHz) data in $CDCl_3$ is illustrated in Table 1. LC-ESI-MS revealed a pseudomolecular ion peak at *m/z* 505 and 503 $[M+H]^+$ and $[M-H]^-$, respectively, corresponding to the molecular formula $C_{26}H_{32}O_{10}$. Different spectra are available in the supplementary data (Figure S1).

3.6. Cytotoxicity assay

MTT assay was carried out as previously described by Saliba et al., 2002 with some modifications. Basically, 100 µL of the tested compound (dissolved in 5% DMSO and RPMI (Roswell Park Memorial Institute) tissue culture medium) were added to each well to reach a final concentration of X ug/mL. Control wells contained two aliquots of 100 µL of tissue culture medium (MEM + fetal bovine serum in a ratio 9:1), 100 µL sterile DMSO (5%) and RPMI tissue culture medium. Following the specified incubation period (24 h) at 37 °C, the wells were washed with PBS (Phosphate Buffered Saline) and the cells were incubated with MTT solution (2 mg/mL) at 100 µL per each well for 1 h at 37 °C. Supernatants were then removed by decantation and the cells were treated with 100 µL of DMSO per each well to dissolve the formazan crystals formed in the viable metabolically active cells. Elutes of the 8 wells of each test isolate were collected and the absorbance was measured at 540 nm. Control wells were similarly treated and the percentage cytotoxicity was calculated employing the following formula [38, 39]

Cytotoxicity % = 1- {A_{540} of test culture/ A_{540} of control culture} × 100

3.7. In silico studies to evaluate COVID-19 inhibitory potential of the isolated compounds

In silico studies were done for the isolated compounds on 2019-nCoV main protease (PDB ID: 7BRP; 1.80 A°), 2019-nCoV spike glycoprotein (PDB ID: 6VSB; 3.46 A°) and ACE2 (PDB ID: 6VW1; 2.68 A°) downloaded from protein data bank (www.pdb.org). This was performed using Discovery Studio 4.5 (Accelrys Inc., San Diego, CA, USA) employing C-Docker protocol as previously described [40]

Binding energy (ΔG) was determined in Kcal/mole using the following equation [41]:

$\Delta G_{binding} = E_{complex} - (E_{protein} + E_{ligand})$ Where;

$\Delta G_{binding}$: The ligand–protein interaction binding energy,

$E_{complex}$: The potential energy for the complex of protein bound with the ligand,

$E_{protein:}$ The protein potential energy alone

E_{ligand}: The ligand potential energy alone

3.8. ADME / TOPKAT prediction

ADME/TOPKAT (absorption, distribution, metabolism, excretion, and toxicity) prediction was performed for the isolated using Discovery Studio 4.5 (Accelrys Inc., San Diego, CA, USA). Aqueous solubility, plasma protein binding prediction (PPB), human intestinal absorption, blood brain barrier penetration (BBB), cytochrome P450 (2D6) and hepatotoxicity level were chosen as ADME descriptors. Meanwhile, carcinogenic effect on male and female rat FDA, ocular and skin irritation, rat oral LD50, Ames mutagenicity and rat chronic LOAEL were selected as toxicity parameters [42].

4. Conclusion

In depth chemical investigation of the ethyl acetate extract of marine fungus *Aspergillus sp.* isolated from the inner tissues of the soft coral *Sinularia* species resulted in the isolation of one new meroterpenoid austalide X in addition to nine known compounds belonging to austalide class, prenylated indole diketopiperazine alkaloids and phthalic acid derivatives. *In vitro* cytotoxic evaluation using MTT assay revealed that most of the examined compounds showed weak to moderate activities with austalide X displaying substantial cytotoxic activity. *In silico* studies on COVID-19 crucial enzymes showed that phthalic acid and its ethyl derivative exerted potent COVID-19 inhibitory potential evidenced by their fitting scores within the active centers of the examined proteins. ADME/TOPKAT showed that most of the isolated compounds displayed reasonable pharmacokinetic, pharmacodynamic and toxicity properties. Thus, it can be concluded that *Aspergillus* sp. could act as a source of drug leads that could prevent cancer and combat COVID-19 infection with promising pharmacokinetic and pharmacodynamic properties

and thus could be incorporated in pharmaceutical dosage forms. However additional *in vivo* studies followed by clinical trials are highly recommended to be conducted on the isolated compounds to confirm the results of in vitro and in silico studies.

Declarations

Availability of Data and Materials

NMR and MS data of the new compound (compound 1) are provided in the supplementary file, other datasets used and/or analysed during the current study are available from the corresponding author on reasonable request.

Acknowledgments

M.S. Elnaggar, A.N.B. Singab, and A.M. Elissawy would like to acknowledge The Science, Technology, and Innovation Funding Authority; STIFA for its financial support through Joint Egyptian Japanese Scientific Cooperation (JEJSC) grant No. 28925 entitled “Chemical biology on innovative biologically active metabolites from endosymbionts in Egyptian marine invertebrates”.

References

1. N.G. Gomes, F. Lefranc, A. Kijjoa, R. Kiss, Can some marine-derived fungal metabolites become actual anticancer agents?, Mar. Drugs, 13 (2015) 3950–3991.
2. R.X. Tan, W.X. Zou, Endophytes: a rich source of functional metabolites, Natural product reports, 18 (2001) 448–459.
3. M.C. Leal, C. Sheridan, R. Osinga, G. Dionísio, R.J.M. Rocha, B. Silva, R. Rosa, R. Calado, Marine microorganism-invertebrate assemblages: Perspectives to solve the “supply problem” in the initial steps of drug discovery, Mar. Drugs, 12 (2014) 3929–3952.
4. V.J. Paul, M.P. Puglisi, Chemical mediation of interactions among marine organisms, Natural product reports, 21 (2004) 189–209.
5. J.F. Imhoff, Natural products from marine fungi—Still an underrepresented resource, Mar. Drugs, 14 (2016) 19.
6. J. Silber, A. Kramer, A. Labes, D. Tasdemir, From discovery to production: biotechnology of marine fungi for the production of new antibiotics, Mar. Drugs, 14 (2016) 137.
7. A.M. Elissawy, M. El-Shazly, S.S. Ebada, A.B. Singab, P. Proksch, Bioactive terpenes from marine-derived fungi, Mar. Drugs, 13 (2015) 1966–1992.
8. M.S. Elnaggar, S.S. Ebada, M.L. Ashour, W. Ebrahim, A. Singab, W. Lin, Z. Liu, P. Proksch, Two new triterpenoids and a new naphthoquinone derivative isolated from a hard coral-derived fungus Scopulariopsis sp, Fitoterapia, 116 (2017) 126–130.

9. A.M. Elissawy, S.S. Ebada, M.L. Ashour, M. El-Neketi, W. Ebrahim, A.B. Singab, New secondary metabolites from the mangrove-derived fungus Aspergillus sp. AV-2, Phytochemistry Letters, 29 (2019) 1–5.
10. M.S. Elnaggar, S.S. Ebada, M.L. Ashour, W. Ebrahim, W.E. Müller, A. Mándi, T. Kurtán, A. Singab, W. Lin, Z. Liu, Xanthones and sesquiterpene derivatives from a marine-derived fungus Scopulariopsis sp, Tetrahedron, 72 (2016) 2411–2419.
11. M.S. Elnaggar, W. Ebrahim, A. Mándi, T. Kurtán, W.E.G. Müller, R. Kalscheuer, A. Singab, W. Lin, Z. Liu, P. Proksch, Hydroquinone derivatives from the marine-derived fungus Gliomastix sp, RSC Advances, 7 (2017) 30640–30649.
12. M. Bai, C.H. Gao, K. Liu, L.Y. Zhao, Z.Z. Tang, Y.H. Liu, Two new benzophenones isolated from a mangrove-derived fungus Penicillium sp, J. Antibiot., 4.
13. F.S. Youssef, M.L. Ashour, A.N.B. Singab, M. Wink, A comprehensive review of bioactive peptides from marine fungi and their biological significance, Mar. Drugs, 17 (2019) 559.
14. R. Zhang, W. He, Y. Wang, J. Zhao, R. Zhou, L. Li, Y. He, S. Cen, L. Yu, New butyrolactone derivatives from the endophytic Fungus Talaromyces sp. CPCC 400783 of Reynoutria japonica Houtt, The Journal of Antibiotics, 74 (2021) 225–232.
15. A.M. Elissawy, S.S. Ebada, M.L. Ashour, F.C. Özkaya, W. Ebrahim, A.B. Singab, P. Proksch, Spiroarthrinols a and B, two novel meroterpenoids isolated from the sponge-derived fungus Arthrinium sp, Phytochemistry letters, 20 (2017) 246–251.
16. Y. Matsuda, I. Abe, Biosynthesis of fungal meroterpenoids, Natural product reports, 33 (2016) 26–53.
17. B. Sontag, N. Arnold, W. Steglich, T. Anke, Montadial A, a cytotoxic metabolite from Bondarzewia montana, J. Nat. Prod., 62 (1999) 1425–1426.
18. T.V. Antipova, K.V. Zaitsev, Y.F. Oprunenko, A.Y. Zherebker, G.K. Rystsov, M.Y. Zemskova, V.P. Zhelifonova, N.E. Ivanushkina, A.G. Kozlovsky, Austalides V and W, new meroterpenoids from the fungus Aspergillus ustus and their antitumor activities, Bioorg. Med. Chem. Lett., 29 (2019) 6.
19. K.J. Kim, J. Lee, W. Wang, Y. Lee, E. Oh, K.H. Park, C. Park, G.E. Woo, Y.J. Son, H. Kang, Austalide K from the Fungus Penicillium rudallense Prevents LPS-Induced Bone Loss in Mice by Inhibiting Osteoclast Differentiation and Promoting Osteoblast Differentiation, Int. J. Mol. Sci., 22 (2021) 12.
20. J.X. Peng, X.M. Zhang, W. Wang, T.J. Zhu, Q.Q. Gu, D.H. Li, Austalides S-U, New Meroterpenoids from the Sponge-Derived Fungus Aspergillus aureolatus HDN14-107, Mar. Drugs, 14 (2016) 9.
21. J. Wang, Y.N. Sang, S.Q. Tang, P. Zhang, A New Austalide from Penicillium sp. SO01, Chem. Nat. Compd., 56 (2020) 670–673.
22. Y. Zhou, A. Mándi, A. Debbab, V. Wray, B. Schulz, W.E. Müller, W. Lin, P. Proksch, T. Kurtán, A.H. Aly, New Austalides from the Sponge-Associated Fungus Aspergillus sp, European Journal of Organic Chemistry, 2011 (2011) 6009.
23. A.E. Dejesus, R.M. Horak, P.S. Steyn, R. Vleggaar, Biosynthesis of austalide-d, a meroterpenoid mycotoxin from aspergillus-ustus, J. Chem. Soc.-Chem. Commun., (1983) 716–718.

24. T.K. Ma, P.J. Parsons, A.G.M. Barrett, Meroterpenoid Synthesis via Sequential Polyketide Aromatization and Radical Anion Cascade Triene Cyclization: Biomimetic Total Syntheses of Austalide Natural Products, J. Org. Chem., 84 (2019) 4961–4970.
25. L.A. Paquette, M.M. Schulze, a unified synthetic strategy for elaboration of the def tricyclic subunit common to the austalide mycotoxins, Heterocycles, 35 (1993) 585–589.
26. L.A. Paquette, T.Z. Wang, M.R. Sivik, enantioselective synthesis of natural (-)-austalide-b, an unusual ortho ester metabolite produced by toxigenic cultures of aspergillus-ustus, J. Am. Chem. Soc., 116 (1994) 2665–2666.
27. F.S. Youssef, E. Alshammari, M.L. Ashour, Bioactive Alkaloids from Genus Aspergillus: Mechanistic Interpretation of Their Antimicrobial and Potential SARS-CoV-2 Inhibitory Activity Using Molecular Modelling, International journal of molecular sciences, 22 (2021) 1866.
28. F. Wang, Y. Fang, T. Zhu, M. Zhang, A. Lin, Q. Gu, W. Zhu, Seven new prenylated indole diketopiperazine alkaloids from holothurian-derived fungus Aspergillus fumigatus, Tetrahedron, 64 (2008) 7986–7991.
29. F. Xie, X.B. Li, J.C. Zhou, Q.Q. Xu, X.N. Wang, H.Q. Yuan, H.X. Lou, Secondary metabolites from Aspergillus fumigatus, an endophytic fungus from the liverwort Heteroscyphus tener (Steph.) Schiffn, Chem. Biodivers., 12 (2015) 1313–1321.
30. T.V. Antipova, K.V. Zaitsev, Y.F. Oprunenko, A. Ya. Zherebker, G.K. Rystsov, M.Y. Zemskova, V.P. Zhelifonova, N.E. Ivanushkina, A.G. Kozlovsky, Austalides V and W, new meroterpenoids from the fungus Aspergillus ustus and their antitumor activities, Bioorganic & Medicinal Chemistry Letters, 29 (2019) 126708.
31. J. Peng, X. Zhang, W. Wang, T. Zhu, Q. Gu, D. Li, Austalides S-U, New Meroterpenoids from the Sponge-Derived Fungus Aspergillus aureolatus HDN14-107, Marine Drugs, 14 (2016) 131.
32. Y. Zhou, A. Debbab, V. Wray, W. Lin, B. Schulz, R. Trepos, C. Pile, C. Hellio, P. Proksch, A.H. Aly, Marine bacterial inhibitors from the sponge-derived fungus Aspergillus sp, Tetrahedron Letters, 55 (2014) 2789–2792.
33. L.A. Paquette, T.-Z. Wang, M.R. Sivik, Enantioselective synthesis of natural (-)-austalide B, an unusual ortho ester metabolite produced by toxigenic cultures of Aspergillus ustus, Journal of the American Chemical Society, 116 (1994) 2665–2666.
34. L.A. Paquette, T.-Z. Wang, M.R. Sivik, Total Synthesis of (-)-Austalide B. A Generic Solution to Elaboration of the Pyran/p-Cresol/Butenolide Triad, Journal of the American Chemical Society, 116 (1994) 11323–11334.
35. H.M. Mengist, T. Dilnessa, T. Jin, Structural basis of potential inhibitors targeting SARS-CoV-2 main protease, Frontiers in Chemistry, 9 (2021).
36. L. Duan, Q. Zheng, H. Zhang, Y. Niu, Y. Lou, H. Wang, The SARS-CoV-2 spike glycoprotein biosynthesis, structure, function, and antigenicity: Implications for the design of spike-based vaccine immunogens, Frontiers in immunology, 11 (2020) 2593.

37. J. Kjer, A. Debbab, A.H. Aly, P. Proksch, Methods for isolation of marine-derived endophytic fungi and their bioactive secondary products, Nature protocols, 5 (2010) 479–490.
38. J. Murakami, K. Kishi, K. Hirai, K. Hiramatsu, T. Yamasaki, M. Nasu, Macrolides and clindamycin suppress the release of Shiga-like toxins from Escherichia coli O157: H7 in vitro, International journal of antimicrobial agents, 15 (2000) 103–109.
39. A.M. Saliba, A. Filloux, G. Ball, A.S. Silva, M.-C. Assis, M.-C. Plotkowski, Type III secretion-mediated killing of endothelial cells by Pseudomonas aeruginosa, Microbial pathogenesis, 33 (2002) 153–166.
40. A.E. Altyar, M.L. Ashour, F.S. Youssef, Premna odorata: Seasonal Metabolic Variation in the Essential Oil Composition of Its Leaf and Verification of Its Anti-Ageing Potential via In Vitro Assays and Molecular Modelling, Biomolecules, 10 (2020) 879.
41. A.A. Janibekov, F.S. Youssef, M.L. Ashour, N.Z. Mamadalieva, New flavonoid glycosides from two Astragalus species (Fabaceae) and validation of their antihyperglycaemic activity using molecular modelling and in vitro studies, Industrial Crops and Products, 118 (2018) 142–148.
42. A. Mollica, G. Zengin, S. Durdagi, R. Ekhteiari Salmas, G. Macedonio, A. Stefanucci, M.P. Dimmito, E. Novellino, Combinatorial peptide library screening for discovery of diverse α-glucosidase inhibitors using molecular dynamics simulations and binary QSAR models, Journal of Biomolecular Structure and Dynamics, 37 (2019) 726–740.

Tables

Table 1 ^{1}H (400 MHz) and ^{13}C (100 MHz) data of **1** and **2** in $CDCl_3$ (δ in ppm, *J* in Hz)

Position	Compound (1)	
	δ_C, type	δ_H (J in Hz)
1	68.2, CH_2	5.14, *s*
2		
3	169.7, C	
4	108.3, C	
5	155.3, C	
6	115.9, C	
7	157.1, C	
8	114.3, C	
9	145.5, C	
10		
11	79.2, C	
12	44.5, CH_2	2.64, *d* (14.5) 2.39, *d* (14.5)
13	102.0, C	
14	92.2, C	
15	86.7, C	
16		
17	118.5, C	
18	69.2, CH	3.80, *dd* (5.5, 0.9)
19	37.7, CH_2	2.15, *dd* (15.9, 0.9) 1.85, *dd* (15.9, 5.5)
20	39.2, C	
21	38.2, CH	3.05, *dd* (7.5, 1.8)
22	17.8, CH_2	2.95, *m*
23	10.9, CH_3	2.06, *s*
24	27.3, CH_3	1.35, *s*
25		4.16, *d* (9.7)

	78.2, CH_2	3.95, *d* (9.7)
26	23.0, CH_3	1.69, *s*
27	19.6, CH_3	0.87, *s*
28	49.1, CH_3	3.53, *s*
29	62.2, CH_3	4.16, *s*

Table 2 Comparative LC/PDA results of *Aspergillus* sp. extracts fermented on rice and beans media

The differences between the secondary metabolites major peaks obtained from both media were written in bold

LC/PDA results (Rice medium) at 254 nm				**LC/PDA results (Beans medium) at 254 nm**			
Peak no.	R.T.	UV (nm)	Area %	Peak no.	R.T.	UV (nm)	Area %
7	**4.2**	**281**	**12.58%**				
				11	**5.9**	**262**	**1.58%**
				14	**11.4**	**255**	**8.32%**
				17	**12.4**	**220, 268**	**1.24%**
13	12.7	228, 260	6.57%	18	12.7	222, 262	2.69%
				19	**13.2**	**227, 260**	**3.13%**
17	16.24	227, 262, 293	1.48%	25	16.7	222, 261, 291	1.95%
18	17.8	294	1.19%	27	17.9	242, 260, 298	1.62%
20	**18.7**	**250**	**1.93%**				
				31	**22.4**	**221, 275**	**6.23%**
26	**22.7**	**251, 290**	**2.13%**				
27	24.06	270	2.05%	32	24.03	230, 270	4.75%
28	**25.5**	**233, 267, 296**	**2.05%**				
31	27.4	228, 267, 300	5.84%	33	27.4	225, 267, 300	3.36%
35	29.7	256	4.60%	35	29.7	259	19.65%
38	**32.8**	**281**	**18.01%**				
40	**35.7**	**281**	**21.2%**				

Table 3 Comparative LC/PDA/MS results of *Aspergillus* sp. extracts fermented on Rice and Beans media.

PDA RT (min)	RICE medium					BEANS medium				
	PDA Peak no.	UV (nm)	Area %	+ESI m/z	-ESI m/z	PDA Peak no.	UV (nm)	Area %	+ESI m/z	-ESI m/z
4.2	*7*	*281*	*12.58%*	*155*						
5.9						*11*	*262*	*1.58%*		*287*
11.4						*14*	*255*	*8.32%*	*199*	
12.4						*17*	*220, 268*	*1.24%*		*329*
12.7	13	228, 260	6.57%	232	230	18	222, 262	2.69%	232	230
13.2						*19*	*227, 260*	*3.13%*		
16.3	*17*	*227, 262, 293*	*1.48%*	*412*						
16.7						*25*	*222, 261, 291*	*1.95%*	*232, 247*	*230, 245*
17.9	18	294	1.19%	169	167	27	242, 260, 298	1.62%	169	
18.7	*20*	*250*	*1.93%*	*427*	*425, 851*					
22.4						*31*	*221, 275*	*6.23%*	-	-
22.7	*26*	*251, 290*	*2.13%*		*426*				-	-
24.05	27	270	2.05%	505	503	32	230, 270	4.75%	505	503
25.5	*28*	*233, 267, 296*	*2.05%*	*394*	*374*					
27.4	31	228, 267, 300	5.84%	209		33	225, 267, 300	3.36%	209	-
29.7	35	256	4.60%		499	35	259	19.65%		499
32.8	*38*	*281*	*18.01%*		*510*				-	-

35.7	*40*	*281*	*21.2%*	*478*	-	-

Table 4 Cytotoxic activity (IC_{50} µg/mL) of compounds isolated from *Aspergillus* sp. against Caco-2 cancer cell lines

Compound	IC_{50} µg/mL
1	51.6
2	57.0
3	126.0
4	32.5
6	105.0
8	51.9
Doxorubicin*	1.25

*** Positive control**

Table 5 Binding energies (ΔG) of the docked compounds expressed in kcal/mole using *in silico* studies within the active centers of 2019-nCoV main protease, 2019-nCoV spike glycoprotein and ACE2

Compounds	2019-nCoV main protease	2019-nCoV spike glycoprotein	ACE2
1	49.34	73.92	61.54
2	59.45	80.08	68.09
3	10.82	35.33	27.48
4	22.15	47.00	40.62
5	22.28	44.72	38.34
6	-4.14	15.62	5.99
7	-9.44	10.56	4.80
8	43.58	65.20	58.61
9	**-21.13**	**-7.61**	**-15.40**
10	**-25.20**	**-12.17**	**-15.86**
2019-nCoV main protease (ligand)	-64.72	ND	ND
2019-nCoV spike glycoprotein (Ligand)	ND	-2.61	ND
ACE2 (Ligand)	ND	ND	-6.65

Positive values indicate unfavorable interaction

ND: Not done

Table 6 Absorption, distribution, metabolism, excretion, and toxicity (ADMET) predictions of isolated compounds from *Aspergillus* sp.

Compounds	Absorption Level	Solubility Level	BBB Level	PPB Level	CPY2D6	Hepatotoxic	PSA-2D	Alog p98
1	0	2	4	True	NI	NT	2.30	121.44
2	0	1	3	True	NI	NT	3.20	100.63
3	1	2	4	False	NI	Tox	3.49	115.08
4	0	2	2	False	NI	Tox	3.84	85.33
5	1	3	4	False	NI	Tox	1.94	135.33
6	1	3	4	False	NI	Tox	0.40	127.74
7	0	3	4	False	NI	Tox	0.81	115.85
8	0	3	4	False	NI	Tox	0.75	121.98
9	0	3	2	True	NI	NT	2.24	52.46
10	0	4	3	False	NI	Tox	1.09	76.23

0, 1, 2, and 3 indicates good, moderate, low and very low absorption, respectively;

0, 1, 2, 3, 4, and 5 indicates extremely low, very low but possible, low, good, optimal, and too soluble, respectively;

0, 1, 2, 3, and 4 denote very high, high, medium, low, and undefined, penetration *via* BBB respectively.

PBB, plasma protein binding, FALSE means less than 90%, TRUE means more than 90%

NI: Non-inhibitor

NT: Non-toxic; Tox., Toxic

PSA 2D: 2D polar surface area

AlogP98 (the logarithm of the partition coefficient between *n*-octanol and water

Table 7 TOPKAT (Toxicity prediction) analysis of the compounds isolated from *Aspergillus* sp. Both Rat oral LD5 and Rat Chronic LOAEL are expressed in g/kg_body_weight

Compounds	Ames prediction	Rat oral LD50	Rat Chronic LOAEL	Skin irritancy	Ocular irritancy	Rat female NTP	Rat Male NTP
1	Non-Mutagen	0.16	0.0038	Mild	None	Non-Carcinogen	Carcinogen
2	Non-Mutagen	0.29	0.0033	Mild	None	Non-Carcinogen	Carcinogen
3	Non-Mutagen	1.14	0.0043	Mild	Mild	Non-Carcinogen	Non-Carcinogen
4	Non-Mutagen	1.43	0.0026	Mild	Mild	Non-Carcinogen	Non-Carcinogen
5	Non-Mutagen	1.34	0.0036	Mild	Mild	Non-Carcinogen	Non-Carcinogen
6	Non-Mutagen	0.82	0.0145	None	Moderate	Non-Carcinogen	Carcinogen
7	Non-Mutagen	0.89	0.0076	Mild	Moderate	Non-Carcinogen	Carcinogen
8	Non-Mutagen	0.56	0.0218	None	Moderate	Non-Carcinogen	Carcinogen
9	Non-Mutagen	9.68	0.9891	Mild	None	Carcinogen	Non-Carcinogen
10	Non-Mutagen	4.05	1.6549	None	Moderate	Carcinogen	Non-Carcinogen

Figures

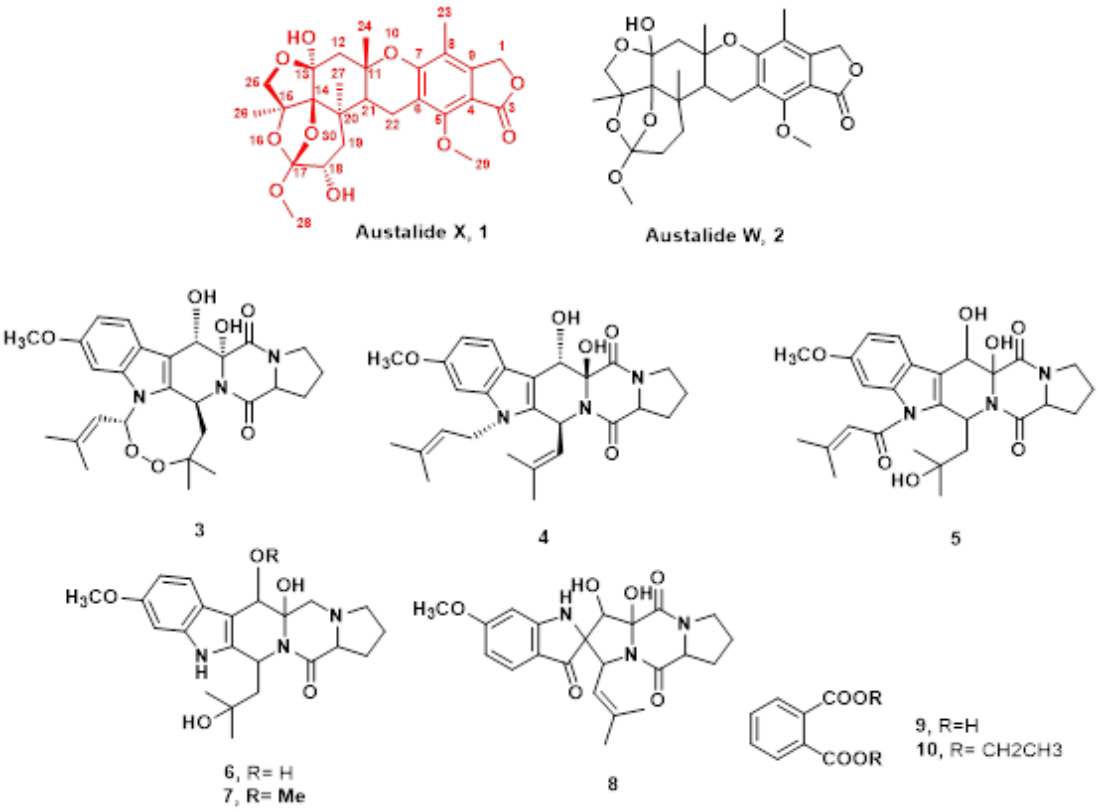

Figure 1

Chemical structures of compounds 1-10 isolated from the ethyl acetate extract of *Aspergillus sp.*

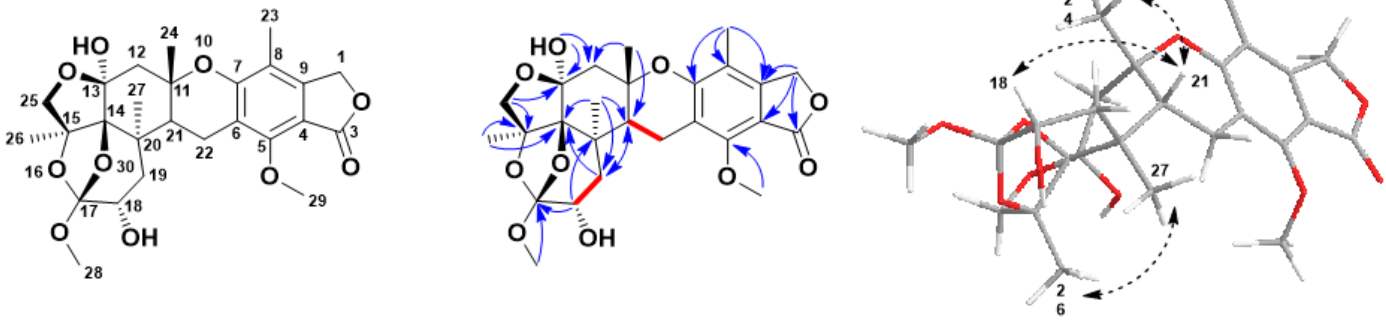

Figure 2

Key COSY, HMBC and NOESY correlations of compound **(1)**

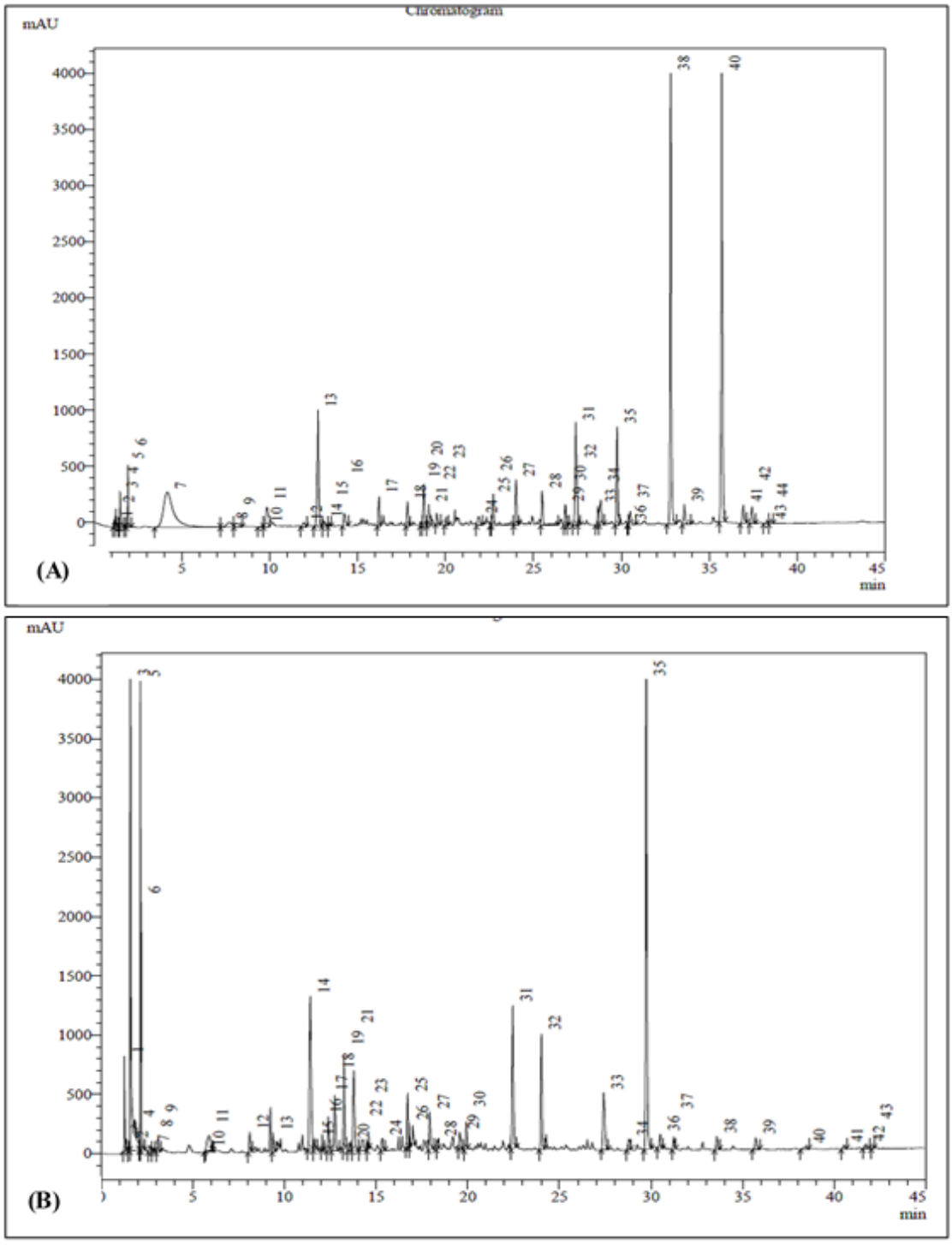

Figure 3

PDA chromatogram of *Aspergillus* sp. extract grown on Rice **(A)** and Beans **(B)** media

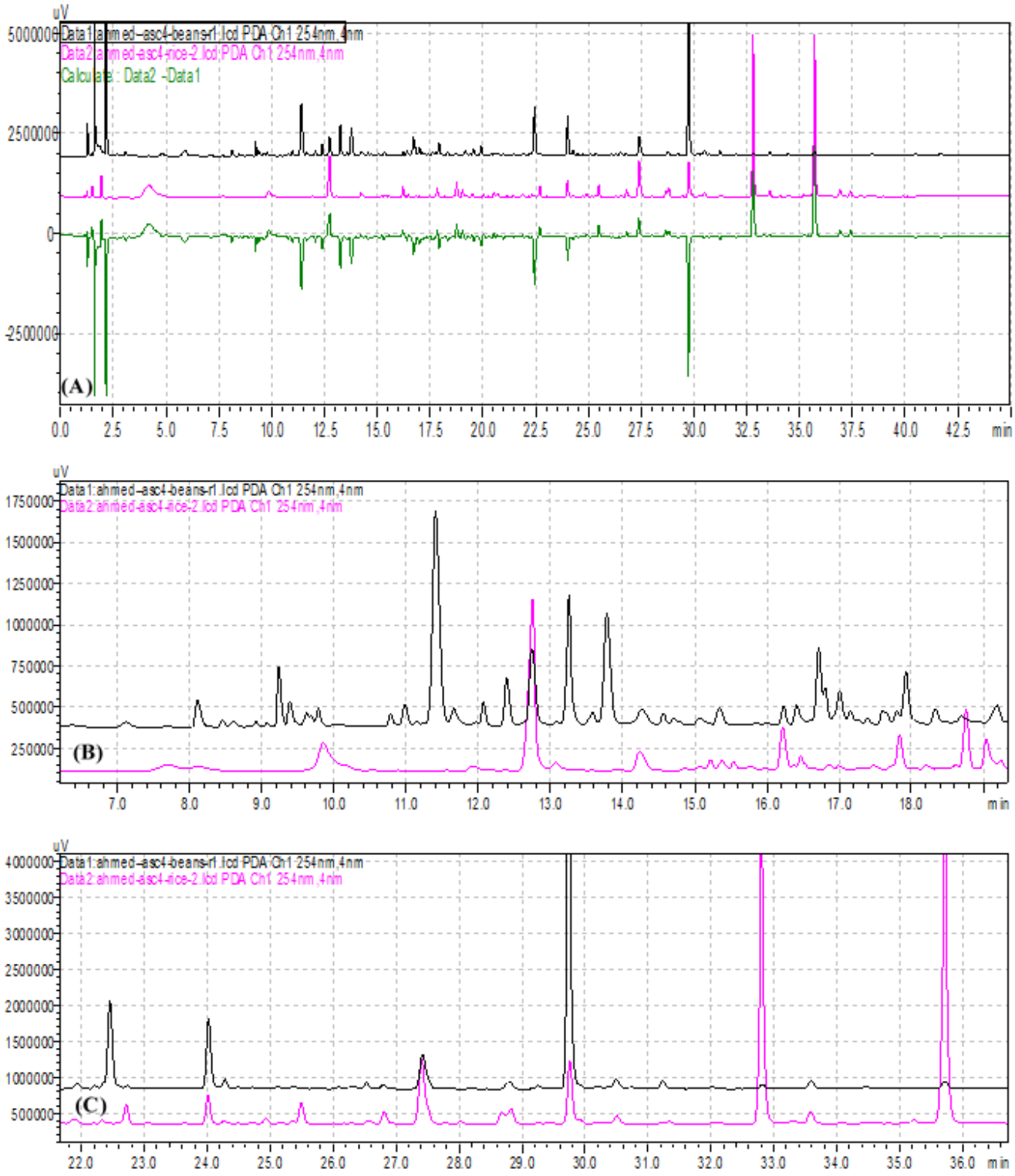

Figure 4

Comparative PDA chromatograms of *Aspergillus* sp. extracts grown on Rice (red) and Beans (black) media **(A),** expanded chromatograms between retention time 7-22 min. **(B) and** expanded chromatograms between retention time 22 -36 min. **(C)**

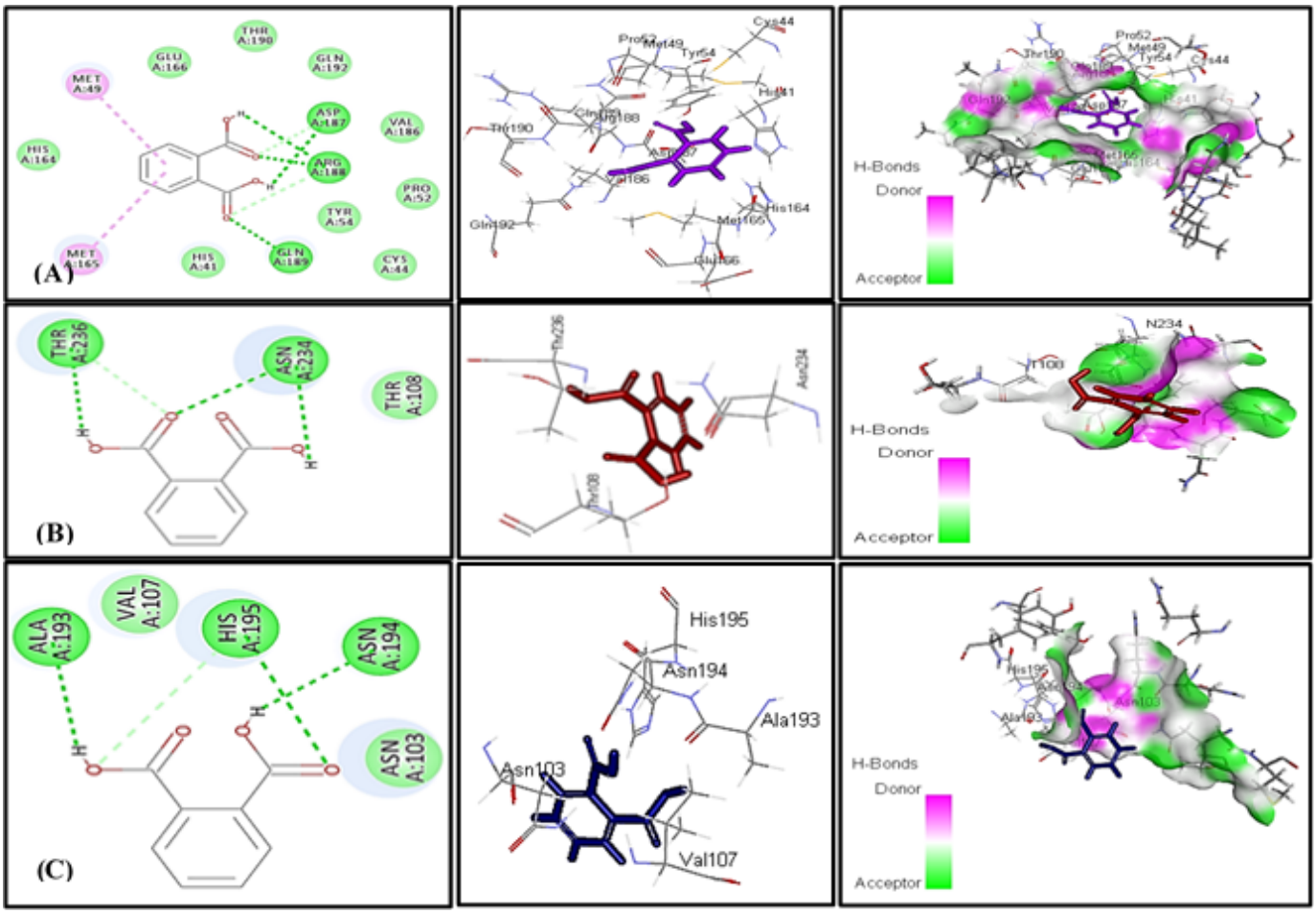

Figure 5

2D, 3D binding mode & active pocket of compound (**10**) within the active site of 2019-nCoV main protease (A), 2019-nCoV spike glycoprotein (B) and ACE2 (C)

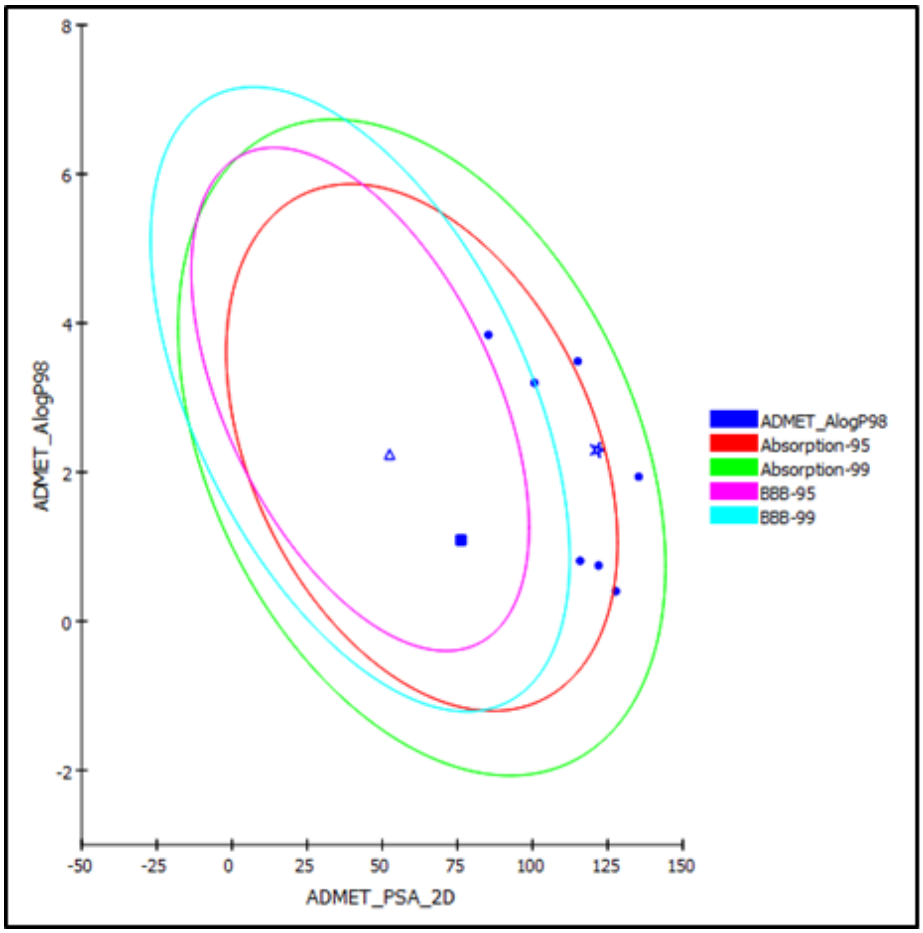

Figure 6

ADMET plot for compound identified from *Aspergillus* sp. displaying the 95% and 99% confidence limit ellipses corresponding to the blood-brain barrier (BBB) and the human intestinal absorption; austalide X (**1**) (star); compound **(9)** (triangle); compound (**10**); (filled square)

Supplementary Files

This is a list of supplementary files associated with this preprint. Click to download.

- supplementary.docx